Journal of Physics: Conference Series **1379** (2019) 012039 doi:10.1088/1742-6596/1379/1/012039

Measurement and compensation of electrostatic forces between conducting surfaces at distances in the micrometer range by means of PTB's nanonewton force facility

Vladimir Nesterov

Physikalisch-Technische Bundesanstalt (PTB), Germany

E-mail: vladimir.nesterov@ptb.de

Abstract. The measurement and compensation of electrostatic forces between conducting surfaces play a major role in various experiments, including measurements of the Newtonian constant of gravitation, measurements of the Casimir force, precision tests of general relativity in space, searches for hypothetical forces (fifth forces), gravity on elementary particles, heating in ion traps, and the physics of Rydberg atoms [1, 2]. Although the actual value of the contact potential was not of direct interest, it was necessary to eliminate it accurately in these experiments in order to avoid residual electrostatic forces that may limit the accuracy and precision of such experiments. We demonstrate how PTB's nanonewton force facility [3, 4] can be used to accurately determine and compensate for the contact potential difference. To measure the contact potential difference as well as the distance between a force sensor and a measured object, a new three-voltage method was developed. A new method of adjusting the parallelism of the plates is also presented. The methods and the results of measuring the contact potential difference and the distance in vacuum are presented for a so-called plane-plane geometry and a ball-plane geometry. Measurements of the temporal and spatial variations of the contact potential difference were performed. Measurements were carried out at distances in the micrometer range between the metallic surfaces. A significant dependence of the contact potential difference on the distance between the conducting surfaces and on the time was found.

1. Introduction

Compared to other surface forces, electrostatic force has a very long range. The contact potential difference is obtained from the difference in the work functions between the conducting surfaces. The work function may vary over a polycrystalline metal surface due to inequivalent crystal facets or due to non-uniform contamination, producing an electrostatically patchy surface (patch effect). It is well known that the work function of a metal surface depends on the crystallographic plane it lies on; as an example, for gold, the work functions are 5.47 eV, 5.37 eV, and 5.31 eV for surfaces in the <100>, <110>, and <111> directions, respectively. The electrostatic potential along a chemically clean metal surface varies along the length of the typical size of surface crystallites, which can vary from the submicron scale to the millimeter scale or larger. Variations on the order of 0.16 V are expected for atomically clean surfaces; however, surface contamination generally seems to reduce these variations to about 10 mV. The baking surfaces in an ultra-high vacuum increased the patch variations, while exposure to air decreased them. It would appear that preferential adsorption of background contaminants is the reason for this, possibly in addition to the migration of existing adsorbates along the surface. For

example, water molecules present on the surface, even in an ultra-high vacuum, have a substantial intrinsic dipole moment. Depending on the coverage and experimental conditions, water on a surface forms different low-dimensional structures ranging from isolated monomers and clusters to one-dimensional (1D) chains and two-dimensional (2D) ordered overlayers. The presence of intrinsic or applied gradient electric fields will lead to an increase in the adsorption (as well as the distortion and migration) of these water structures. Migration and distortion can also occur with surface crystallites. This leads to a change in the distribution of charges and potentials on the surface. A significant temporal dependence of the contact potential difference between the metallic surfaces at distances in the micrometer range has been reported in [7]. Surface electric noise, i.e., the non-uniform and non-stationary distribution of charges and potentials on a surface, poses a great experimental challenge in modern precision force measurements. In this paper, we present an improved version of PTB's nanonewton force facility, which was first published in [3, 4]. The facility is based on a disc pendulum with an electrostatic control system that reduces the stiffness of the pendulum as well as its deflection from a selected position. The improvement of this facility includes a new electrostatic control system in order to generate an electrostatic compensation force and to reduce the angular oscillation of the disc pendulum in a high vacuum. For example, the angular movements of the disc pendulum have been reduced from 10^{-2} rad to $2 \cdot 10^{-7}$ rad in a vacuum of 10^{-6} mbar. To control the mutual arrangement of the upper edges of the plates, a method analogous to confocal laser scanning microscopy (CLSM) was used. The facility is able to measure horizontal forces in the range below 1 µN with a resolution below 5 pN and an uncertainty below 2.7 % for a measured force of 1 nN at a measurement duration of about 20 s [4]. We demonstrate the possibility of using the nanonewton force facility to accurately determine the contact potential difference. To measure the contact potential difference as well as the distance between a force sensor and a measured object, a new three-voltage method was developed. This method makes it possible to compensate for the contact potential difference in real time. For plane-plane geometry and plane-ball geometry, which will be described later, the method used to measure the contact potential difference in a vacuum and the measurement results are presented below. A new method of adjusting the parallelism of the plates (so-called plane-plane geometry) is presented. Measurements of the temporal and spatial variations of the contact potential difference were performed. A significant dependence of the contact potential difference on the distance between the conducting surfaces was found.

2. New design of the nanonewton force facility

The facility consists of a measuring part and an identical reference part in order to reduce thermal drift and seismic noise [3, 4]. The new functional diagram of the measuring part is presented in figure 1. The facility is based on a disc pendulum with electrostatic reduction of its deflection and stiffness in the X-direction. The facility uses a disc pendulum (1) between two electrodes (2) with an electrostatic control system for force measurement. The disc pendulum is made of gold-coated silicon plates (size 30 mm x 30 mm, thickness T_p = 0.425 mm) that are suspended on two gold-coated tungsten wires (1d) (d_w = 10 ± 1 µm in diameter and approx. 424 mm in length). The deflection of the pendulum due to a force is measured by means of an interferometer (8) (attocube FPS3010). The facility can measure horizontal forces in the range below 1 µN, with a resolution below 5 pN and an uncertainty of 2.7 % down to a measured force of 1 nN at a measuring duration of about 20 s [4]. One of the main objectives of the new upgrades was the modification of the disc pendulum design to achieve greater flexibility. A new measuring disc-pendulum was developed wherein a rod (1a) is mounted horizontally through a hole in the center of the pendulum; a gold-coated silicon plate – the "sensor plate" (1b) (size 20 mm x 20 mm, thickness 0.425 mm) – is attached to one side of the rod and a counterbalance (1c) to the other side. The rod (1a) is made of Zerodur with a coefficient of thermal expansion of less than 10^{-8} K^{-1}. To ensure electrical conductivity and to eliminate static charges, all elements are coated with a 100 nm gold layer. The main source of measurement uncertainty and instability in a high vacuum is the free angular oscillations of the disc pendulum around the pendulum's main axes. Such oscillations have a high quality factor and can achieve amplitudes of 10^{-2} rad. To detect these oscillations, a laser beam (9) is reflected

from one end of the rod (1a) onto a quadrant photodiode (10). Each of the electrodes (2) consists of four segments that can be controlled individually by using the signals from the quadrant photodiode (10). The angular oscillations are compensated by means of two additional independent electrostatic control systems, the first of which compensates for angular oscillations relative to the Y-axis, and the second of which compensates for the angular oscillations relative to the Z-axis.

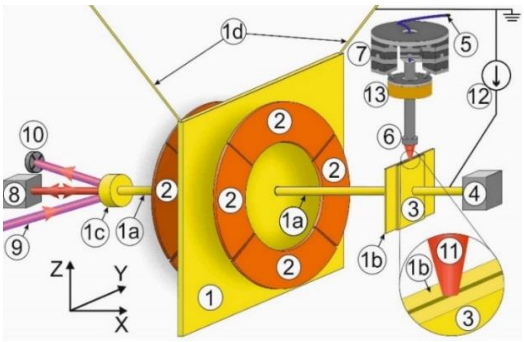

Figure 1. Functional diagram of the measuring part of the nanonewton force facility: (1) gold-coated disc pendulum; (1a) gold-coated Zerodur rod; (1b) sensor plate; (1c) counterbalance; (1d) disc pendulum suspension (thin gold-coated tungsten wires); (2) outer conductive electrodes (each consists of four segments); (3) probe plate; (4) 6D positioner; (5) single mode fiber laser system; (6) focusing optical system; (7) 6D positioner (Hexapod); (8) interferometer; (9) laser beam; (10) quadrant photodiode; (11) focused laser beam; (12) voltage source; (13) rotator.

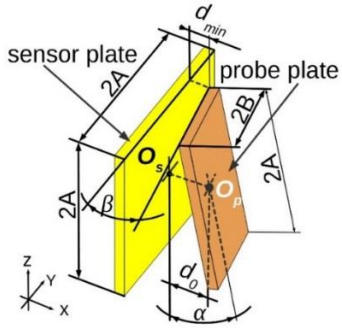

Figure 2. The location of the sensor (1b) and of the probe plates (3) (*2A* = 20 mm; *2B* = 4 mm).

The angular oscillations can be reduced by several orders of magnitude. For example, in a vacuum of 10^{-6} mbar, the angular oscillations of the disc pendulum have been reduced from 10^{-2} rad to $2 \cdot 10^{-7}$ rad. The quadrant photodiode with the two electrostatic control systems also makes it possible to measure the torque that acts on the disc pendulum (sensor plate). The nanonewton force facility contains three independent electrostatic control systems. Each of these systems is a PID (proportional-integral-derivative) real-time control system with a sampling period of about 1 µs. Control voltages are applied independently to each of the eight segments from the FPGA card. The FPGA card operates under the control of a real-time system and provides voltages from 0 V to 10 V. For a so-called plane-plane geometry, a gold-coated silicon plate (size 20 mm x 4 mm, thickness 0.425 mm) was used as a probe plate (3). This plate is attached and moved using a 6D positioner (4). A slit whose width is in the sub-micrometer to millimeter range can be created between the probe plate (3) and the sensor plate (1b). The electrical voltages may be applied between the plates (3, 1b) by means of the voltage source (12). The electrostatic force arises between the sensor plate (1b) and the probe plate (3). The location of the sensor plate and of the probe plate is presented in figure 1.

This force is measured by means of the nanonewton force facility. To control the arrangement of the upper edges of the plates (3, 1b), a method analogous to confocal laser scanning microscopy (CLSM) is used. The light is provided by a single mode fiber laser system with a wavelength of $\lambda = 1550$ nm (5) and an output power P ($0 \text{ W} < P < 2 \text{ W}$). The laser beam is focused by means of an optical system (6) until it forms a spot radius of about $\omega = 4$ µm (11) on the upper edges of the plates. The whole optical system is mounted on a compact 6D positioner called a hexapod (7). The hexapod is used as a scanning system. The power of the radiation reflected from the upper edges of the plates and returned to the single mode fiber is measured. For the so-called plane-ball geometry, the probe plate (3) is replaced with a ball (hemisphere).

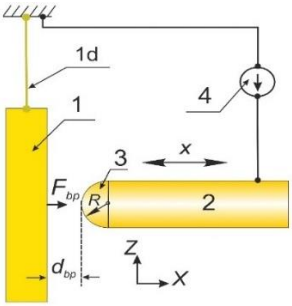

Figure 3. Ball-plane geometry: (1) disc pendulum (sensor plate); (1d) disc pendulum suspension (thin gold-coated tungsten wires); (2) movable mounting rod; (3) probe ball; (4) voltage source.

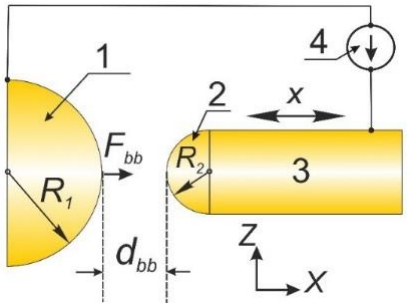

Figure 4. Ball-ball geometry: (1) sensor ball; (2) probe ball; (3) movable mounting rod; (4) voltage source.

3. New three-voltage method

In this section, we first consider a so-called plane-plane geometry (Figure 1 and 2), which is a most complicated case. To measure the contact potential difference δu as well as the distance d_0 between the center of the sensor plate (1b) and the center of the probe plate (3) (Figure 1 and 2), a new three-voltage method was developed (first presented in [5]). Let us assume that an electrical voltage u exists between the sensor plate and the probe plate. The beginning of the Cartesian coordinate system is located in the center of the sensor plate at the point O_s (Figure 2). Let us assume that the centers of the plates (points O_s and O_p) are located on the X-axis. The required position of the plates is controlled by means of confocal laser scanning microscopy (CLSM). The angles of rotation between the plates are α (relative Y-axis) and β (relative Z-axis). We will assume that the dimensions of the *2A* and *2B* plates considerably exceed the distance d_0 between them ($d_0 << 2A$, $d_0 << 2B$). In this case, the edge effects can be neglected. Assuming that $\alpha << 1$ and $\beta << 1$, the electrostatic force $F(u)$ between the plates can be described by the following expressions:

$$F(u) = \frac{1}{2} \cdot \frac{\partial C_{pp}}{\partial d_0} \cdot u^2 = \frac{\varepsilon_0 \cdot u^2}{2} \cdot \int_{-A}^{A} dz \int_{-B}^{B} \frac{dy}{(d_0 - \alpha z - \beta y)^2} = \frac{T_{pp} \cdot u^2}{D(d_0)^2} \ , \tag{1}$$

$$T_{pp} = 2 \cdot \varepsilon_0 \cdot A \cdot B \ , \tag{2}$$

$$D(d_0)^2 = {d_0}^2 - (\alpha \cdot A)^2 - (\beta \cdot B)^2 \ , \tag{3}$$

where C_{pp} is the capacity between the plates, ε_0 is the vacuum permittivity.

The voltages u_0, $u_1$and u_2 are applied between the plates by means of the voltage source (12). At the same time, the forces $F(u_0)$, $F(u_1)$, and $F(u_2)$ are measured. Taking the contact potential difference δu into account, these measured forces can be written as:

$$F(u_0) = \frac{T_{pp} \cdot (u_0 + \delta u)^2}{D(d_0)^2} + \delta F \ , \tag{4}$$

$$F(u_1) = \frac{T_{pp} \cdot (u_1 + \delta u)^2}{D(d_0)^2} + \delta F \ , \tag{5}$$

$$F(u_2) = \frac{T_{pp} \cdot (u_2 + \delta u)^2}{D(d_0)^2} + \delta F \ , \tag{6}$$

where δF is the offset force (any force independent of the applied voltage).

Solving the system of equations (4-6), the contact potential difference δu and the parameter $D(d_0)^2 = ({d_0}^2 - (\alpha \cdot A)^2 - (\beta \cdot B)^2)$ are represented by means of the following expressions:

$$\delta u = -\frac{F(u_0)\cdot(u_2^2-u_1^2)+F(u_1)\cdot(u_0^2-u_2^2)+F(u_2)\cdot(u_1^2-u_0^2)}{2\cdot(F(u_0)\cdot(u_2-u_1)+F(u_1)\cdot(u_0-u_2)+F(u_2)\cdot(u_1-u_0))}\ , \tag{7}$$

$$D(d_0)^2 = \frac{T_{pp}\cdot((u_1+\delta u)^2-(u_0+\delta u)^2)}{F(u_1)-F(u_0)}, \tag{8}$$

$$D(d_0)^2 = {d_0}^2 - L^2\ , \quad L^2 = (\alpha\cdot A)^2 + (\beta\cdot B)^2\ . \tag{9}$$

To determine the distance d_0, the probe plate (3) (Figures 1 and 2) is displaced in the X-direction by a known distance Δ. Using the three-voltage method and the equations (7, 8) at a distance d_0 (unknown) and at a distance (d_0 + Δ), the parameters $D(d_0)^2$ and $D(d_0+\Delta)^2$ are determined. Using equation (9), the distance d_0 is calculated by means of the following expression:

$$d_0 = \frac{D(d_0+\Delta)^2 - D(d_0)^2-\Delta^2}{2\cdot\Delta} \tag{10}$$

When the distance d_0 is known and equation (9) is used, the parameter L and the minimum distance between the plates d_{min} (Figure 2) are given by the following equations:

$$L^2 = (\alpha\cdot A)^2 + (\beta\cdot B)^2 = {d_0}^2 - D(d_0)^2\ , \tag{11}$$

$$d_{min} = d_0 - L\ . \tag{12}$$

Note that the method can be easily expanded to include a ball-plane geometry (Figure 3) and a ball-ball geometry (Figure 4). Using of the so-called proximity force theorem (PFT) [6], the electrostatic force F_{bp} of the ball-plane geometry is given by means of the equations:

$$F_{bp} = T_{bp}\cdot\frac{u^2}{d_{bp}}, \qquad T_{bp} = \pi\cdot\varepsilon_0\cdot R\ , \tag{13}$$

where R is the radius of the ball, d_{bp} is the distance between the ball and plane (Figure 3). Replacing T_{pp} with T_{bp} and $D(d_0)^2$ with d_{bp} in equations (4-6) and using equations (8,13) the distance d_{bp} is calculated by means of the expression:

$$d_{bp} = \frac{T_{bp}\cdot((u_1+\delta u)^2-(u_0+\delta u)^2)}{F(u_1)-F(u_0)}\ . \tag{14}$$

Using the PFT, the electrostatic force F_{bb} of the ball-ball geometry is given by means of the equations:

$$F_{bb} = T_{bb}\cdot\frac{u^2}{d_{bb}}, \qquad T_{bb} = \pi\cdot\varepsilon_0\cdot\frac{R_1\cdot R_2}{(R_1+R_2)}, \tag{15}$$

Where R_1 and R_2 are the radiuses of the balls, d_{bb} is the distance between the balls (Figure 4). Replacing T_{pp} with T_{bb} and $D(d_0)^2$ by d_{bb} in equations (4-6) and using equations (8,15), the distance d_{bb} is calculated by means of the expression:

$$d_{bb} = \frac{T_{bb}\cdot((u_1+\delta u)^2-(u_0+\delta u)^2)}{F(u_1)-F(u_0)}\ . \tag{16}$$

The contact potential differences δu of the ball-plane geometry and the ball-ball geometry, as well as those of the plane-plane geometry, are given by equation (7). Note that the contact potential difference δu determined from equation (7) does not depend on the calibration of the force meter used. Note also that equation (7) can be used for any given geometry and relative position of the conductive surfaces.

4. Adjustment of the parallelism of the plates

The parameter L characterizes the degree of the parallelism of the probe plate (3) relative to the sensor plate (1b). The parallelism of the plates corresponds to the zero value of the parameter L. Another method of setting the parallelism of the plates is to minimize the torque applied to the sensor plate (1b) by the probe plate (3) (Figures 1 and 2). Using CLSM (Section 2), an angle of $\beta < 10^{-4}$ rad between the plates is achieved in practice. To simplify the calculations, we assume that the angle β between the plates

is zero. In this case, the torque $M_Y(\alpha)$ applied to the sensor plate (1b) by the probe plate (3) can be written as

$$M(\alpha)_Y = \int_{-A}^{A} \frac{\varepsilon_0 \cdot u^2 \cdot B \cdot z \cdot dz}{(d_0 - \alpha \cdot z)^2} = \frac{4 \cdot \varepsilon_0 \cdot u^2 \cdot A^3 \cdot B}{3 \cdot d_0^3} \cdot \alpha \cdot \left(1 + \frac{6}{5} \cdot \left(\frac{\alpha \cdot A}{d_0}\right)^2 + O\left(\left(\frac{\alpha \cdot A}{d_0}\right)^4\right)\right). \quad (17)$$

If the angle α between the plates is small ($\alpha \cdot A << d_0$), it follows from equation (17) that the dependence of the torque $M_Y(\alpha)$ on the α is linear. The parallelism of the plates ($\alpha = 0$) corresponds to the zero value of the torque $M_Y(\alpha)$. After parallelism of the plates has been achieved, the desired angles of inclination α and β can be set by turning and displacing the probe plate (3) by means of the 6D positioner (4).

5. Measurements

Figures 5 and 6 show the measurements of the contact potential difference δu and the distance d_0 between the plates (1b, 3) for plane-plane geometry by means of the new three-voltage method. The voltages $u(t)$ are applied between the plates (1b, 3) by means of the voltage source (12). Figures 7 and 8 show the measurements of the contact potential difference δu (blue solid line) and the distance d_0 (brown solid line) between the plates (1b, 3) for plane-plane geometry by means of the new three-voltage method, when distance changes cyclically. To change the distance between the plates, the probe plate (3) is moved stepwise relative to the sensor plate (1b) with a step size of 20 nm and a time step of 90 s. During each step of the probe plate with a time step of $\tau_p = 90$ s, the voltage changes three times with a basic time interval of $\tau_u = 30$ s. The mean values of the force are calculated from the signal measured after it has passed a Bessel low-pass filter (0.05 Hz, 12th order) in the interval from 21 s to 30 s after the start of the voltage interval. During each step, the contact potential difference (compensation voltage) δu and the distance d_0 are calculated. Thus, the contact potential difference δu using the three-voltage method is measured and compensated to zero for each step of the probe plate. The measurements were carried out in a vacuum of about $2 \cdot 10^{-7}$ mbar.

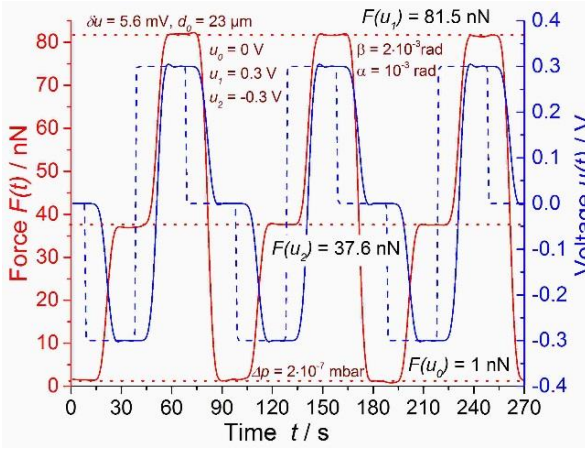

Figure 5. Demonstration of the new three-voltage method without compensation of the contact potential difference: applied voltage = blue dashed line; applied voltage after the low-pass filter = blue solid line; measured force after the low-pass filter = red line.

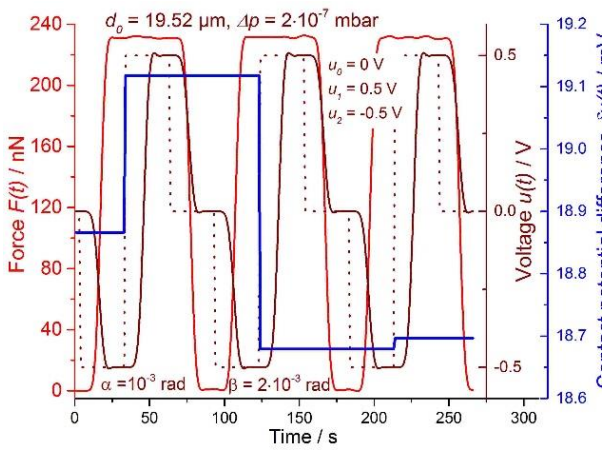

Figure 6. Demonstration of the new three-voltage method with the contact potential difference compensation: applied voltage = brown dashed line; applied voltage after the low-pass filter = brown solid line; measured force = red line; measured and compensated contact potential difference = blue solid line.

The probe plate (3) was tilted around the vertical Z-axis ($\beta = 2 \cdot 10^{-3}$ rad) and the horizontal Y-axis ($\alpha = 10^{-3}$ rad) relative to the sensor plate (1b). The measured contact potential difference $\delta u(t)$ versus time and its power spectral density are presented in figure 9 (vacuum $\Delta p = 2 \cdot 10^{-7}$ mbar). In this experiment, the distance between the plates $d_0 = 23.4$ µm ($d_{min} = 1$ µm) was constant.

For ball-plan geometry, the probe ball (3) (hemisphere with a radius $R = 4.2$ mm) is moved stepwise relative to the sensor plate (1) (Figure 3) with a step size of 5 nm and a time step of 60 s. The measured contact potential difference δu and temperature variations of the facility versus the distance d_{bp} in a vacuum $\Delta p = 0.1$ mbar are presented in figure 10.

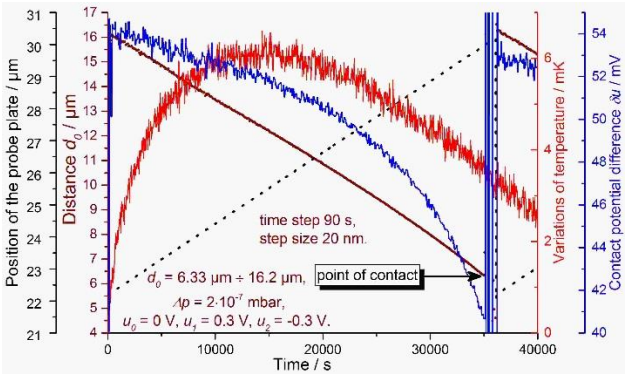

Figure 7. Measurements of the contact potential difference δu (blue solid line) and the distance d_0 (brown solid line) between the plates (1b, 3) for plane-plane geometry when distance changes cyclically: position of the probe plate = black dashed line; temperature variations of the facility = red line.

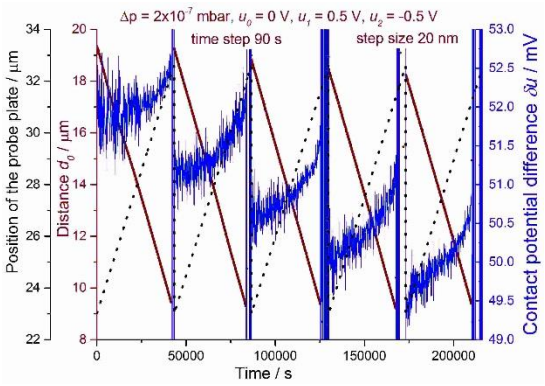

Figure 8. Measurements of the contact potential difference δu (blue solid line) and the distance d_0 (brown solid line) between the plates (1b, 3) for plane-plane geometry when distance changes cyclically (5 cycles): position of the probe plate = black dashed line.

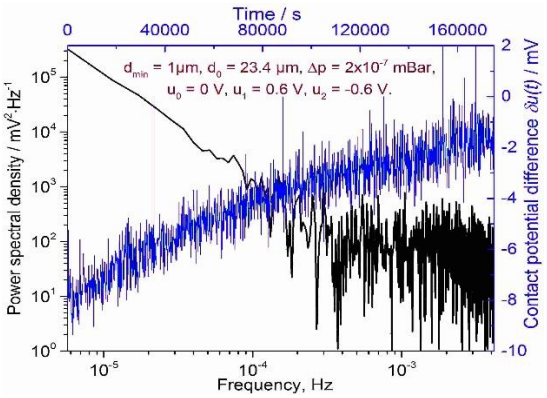

Figure 9. Measured contact potential difference $\delta u(t)$ versus time (blue line) and its power spectral density (black line) in a vacuum $\Delta p = 2 \cdot 10^{-7}$ mbar for plane-plane geometry.

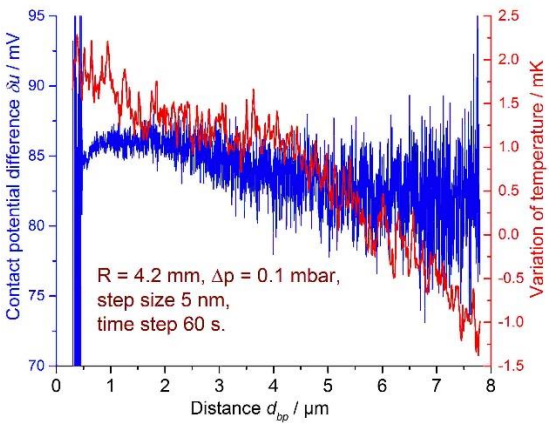

Figure 10. Measured contact potential difference δu (blue line) and temperature variations of the facility (red line) versus the distance d_{bp} in a vacuum $\Delta p = 0.1$ mbar for ball-plane geometry.

It should be noted that there is only a weak correlation of the contact potential difference δu with the temperature variations of the facility. It should also be noted that there is a strong variability in the

dependences of the contact potential difference δu versus the distance d_0 (Figures 7 and 8). This behavior can be explained by structural surface changes as a result of the action of electric fields arising between the surfaces. These changes may include the structure of gold clusters that cover the surfaces. Temporary changes in the contact potential difference in some experiments exceeded 100 mV per day. Changes in the contact potential difference δu should be compensated during precision measurements.

Acknowledgements
This work was supported by the Deutsche Forschungsgemeinschaft (DFG NE 1550/2-1 and DFG NE 1550/2-2). I want to express my gratitude to my grandson Roman for the constant interest in my work.

References
[1] Behunin R O, Dalvit D A R, Decca R S and Speake C C 2014 *Phys. Rev. D* **89**, 051301(R)
[2] Sushkov A O, Kim W J, Dalvit D A R and Lamoreaux S K 2011 *Phys. Rev. Lett.* **107** 171101
[3] Nesterov V 2007 *Meas. Sci. Technol.***18**, 360
[4] Nesterov V, Belai O, Nies D, Buetefisch S, Mueller M, Ahbe T, Naparty D, Popadic R and Wolff°H 2016 *Metrologia* **53** 1031
[5] Nesterov V, Nies D, Belai O, Buetefisch S, Kirchhoff J, Mueller M and Brand U 2018 *Proc. Int. Conf. CPEM* (Paris) p 950
[6] Blocki J, Randrup J, Swiatecki W J and Tsang C F 1977 *Annals of Physics* **105** 427-462
[7] Robertson N A, Blackwood J R, Buchman S, Byer R L, Camp J, Gill D, Hanson J, Williams S and Zhou P 2006 *Classical Quant. Grav.* **23** 2665-80